Univerzita Karlova

Přírodovědecká fakulta

Studijní program: Chemie

Studijní obor: Chemie

Soňa Mesíková

Příprava hybridních nanočástic založených na interakci blokových polyelektrolytů s atypickými ionty

Preparation of hybrid nanoparticles based on interaction of block polyelectrolytes with atypical ions

Bakalářská práce

Školitel: doc. RNDr. Pavel Matějíček, Ph.D.

Konzultant: Ing. Mariusz Marcin Uchman, Ph.D.

Praha, 2020

Prohlášení:

Prohlašuji, že jsem závěrečnou práci zpracovala samostatně a že jsem uvedla všechny použité informační zdroje a literaturu. Tato práce ani její podstatná část nebyla předložena k získání jiného nebo stejného akademického titulu.

V Praze, 05.08.2020

Podpis

Abstrakt

Bakalářská práce se zabývá asociačním chováním kationtových dvojblokových kopolymerů poly(2-vinyl pyridin)-*b*-poly(ethylen oxid), P2VP-*b*-PEO, a poly(ethylen oxid)-*b*-poly(2-(N, N, N′, N′-tetramethyl guanidin) ethyl akrylát), PEO-*b*-PGEA, s *closo*-dodekaborátovým aniontem, $[B_{12}H_{12}]^{2-}$, ve vodných roztocích. Vznik stabilních nanočástic PEO-*b*-PGEA/$[B_{12}H_{12}]$ byl pozorován pomocí statického a dynamického rozptylu světla a ^{1}H NMR spektroskopie. Tvar těchto částic byl dále určen pomocí mikroskopie cryo-TEM jako kulovitý. Provedené NMR experimenty naznačují, že struktura nanočástic tvořených studovanými blokovými kopolymery s dodekaborátem lze popsat modelem micely s jádrem a koronou. Molární hmotnost micel a tomu odpovídající agregační číslo systému PEO-*b*-PGEA/$[B_{12}H_{12}]$ bylo změřeno ve vodě a v 0.156 M vodném roztoku NaCl pomocí standardní metody Zimmových sítí. Pro tyto účely byla experimentálně stanovena hodnota inkrementu indexu lomu pomocí refraktometru. Studované nanočástice mají potenciál jako nosiče bóru v medicíně.

Abstract

The Thesis deals with the co-assembly behaviour of cationic diblock copolymers poly(2-vinyl pyridine)-*b*-poly(ethylene oxide), P2VP-*b*-PEO, and poly(ethylene oxide)-*b*-poly(2-(N, N, N′, N′-tetramethyl guanidinium) ethyl acrylate), PEO-*b*-PGEA, with *closo*-dodecaborate anion, $[B_{12}H_{12}]^{2-}$, in aqueous solutions. Formation of stable PEO-*b*-PGEA/$[B_{12}H_{12}]$ nanoparticles was investigated by static and dynamic light scattering and ^{1}H NMR spectroscopy, and they were visualized as spherical nanoparticles by cryo-TEM imaging. According to the NMR results, both studied diblock copolymers form core-corona micelles with dodecaborate. The micellar molar mass and the aggregation number of PEO-*b*-PGEA/$[B_{12}H_{12}]$ micelles were obtained in water and 0.156 M NaCl solution by standard Zimm method. For this, refractive index increment was evaluated by refractometer. The studied nanoparticles are promising for the boron delivery in medicine.

Abbreviations

ABCCs - anionic boron cluster compounds

AIBN - 2,2′-Azobis(2-methylpropionitrile)

BEA - 2-bromethyl acrylate

BNTC - boron neutron capture therapy

CMC - critical micelle concentration

CONTIN - constrained inverse Laplace transform routine

Cryo-TEM - cryogenic transmission electron microscopy

DLS - dynamic light scattering

DMF - N,N-Dimethylformamide

LS - light scattering

NMR - nuclear magnetic resonance

P2VP - poly(2-vinyl pyridine)

PBEA - poly(2-bromethyl acrylate)

PEO - poly(ethylene oxide)

PGEA - poly(2-(N,N, N′, N′-tetramethyl guanidinium) ethyl acrylate)

RAFT - reversible addition-fragmentation chain transfer polymerization

RDRP - reversible deactivation radical polymerization

SAXS- Small Angle X-ray scattering

SLS - static light scattering

t-BuOH - *tert*-butanol

TTCA - S-1-Dodecyl-S′-(R,R′-dimethyl-R′′-acetic acid) trithiocarbonate

Content

1. Introduction 1
2. Overview of the literature 3
   2.1. Reversible addition-fragmentation chain transfer polymerization 3
   2.2. Block copolymer architecture 4
   2.3. Self-assembly of amphiphilic diblock copolymers in aqueous solutions 4
   2.4. Coassembly of diblock copolymers 5
   2.5. Techniques for micelle-structure characterization 6
      2.5.1. Light scattering 6
      2.5.2. Nuclear magnetic resonance 10
   2.6. Applications of polymer micelles 11
      2.6.1. Drug delivery 11
      2.6.2. Boron neutron capture therapy 12
3. Aims of the thesis 13
4. Materials and used methods 14
   4.1. Used polymers and other reagents 14
   4.2. Micelles preparation 15
   4.3. Refractive increment index 16
   4.4. Static and dynamic light scattering 16
   4.5. Nuclear magnetic resonance 17
   4.6. Cryo-TEM 17
5. Results and discussion 18
   5.1. Synthesis of PEO_{114}-*b*-$PGEA_{23}$ 18
   5.2. Micelle characterization 19
      5.2.1. Static and dynamic light scattering 19
      5.2.2. Nuclear magnetic resonance 25
      5.2.3. Cryo-TEM 27
6. Conclusion 28
7. References 29

1. Introduction

The self-assembly of block copolymers and surfactants belongs to the most intensively studied topics in nanochemistry for over the decades. The key point is to understand the principles of assembly of nano-sized building block that could be utilized in preparation of nanomaterials for numerous applications such as nanomedicine, nanoelectronics, nanolithography, catalysis, etc. While the basic principles of self-assembly of block copolymers are already well understood, new systems going beyond the already established theories are continuously synthetized and investigated. One of the promising approaches is a producing of nanostructures by coassembly of hydrophilic block copolymers with ions, ionic surfactants and other nano-blocks leading to hybrid nanoparticles of unique properties and morphology.

In this Thesis, the coassembly of cationic block copolymers with anionic boron cluster compounds was investigated. We used poly(2-vinyl pyridine)-*b*-poly(ethylene oxide), P2VP-*b*-PEO, and poly(ethylene oxide)-*b*-poly(2-(N, N, N′, N′-tetramethyl guanidinium) ethyl acrylate), PEO-*b*-PGEA, diblock copolymers in water solutions and studied the formation of hybrid nanoparticles after their mixing with sodium *closo*-dodecaborate, $Na_2[B_{12}H_{12}]$. While dodecaborate salts are usually highly water soluble, almost nanometer size and unique chemical composition differentiate dodecaborate dianion from classical inorganic ions. Size, shape and the mechanism of formation of the nanoparticles were studied by static and dynamic light scattering and NMR spectroscopy complemented by cryo-TEM imaging.

The Thesis is a part of long-term investigation of self- and co-assembly of boron cluster compounds in Soft Matter research team, thus, it would not be possible without cooperation with the team member and other colleagues: PEO-PGEA diblock copolymers were synthetized by PhD-student Jianwei Li, NMR spectra were measured with help of PhD-student Roberto Fernandez-Alvarez, and cryo-TEM imaging was performed by Sami Kereïche (Institute of Cellular Biology and Pathology, First Faculty of Medicine, Charles University). I prepared all the solutions, performed light scattering and refractive index measurements, evaluated the experimental data and calculated refractive index increment.

The financial support of the Czech Science Foundation 19-13458S is gratefully acknowledged.

The Thesis also contributed to the project that has been very recently published: Jianwei Li, Olga Janoušková, Roberto Fernandez-Alvarez, Soňa Mesíková, Zdeněk Tošner, Sami Kereïche, Mariusz Uchman and Pavel Matějíček, “Designed Boron-Rich Polymeric Nanoparticles Based on Nano-Ion Pairing for Boron Delivery” Chemistry–A European Journal, 2020, doi: 10.1002/chem.202001699, IF = 4.857. The manuscript is attached to the Thesis.

2. Overview of the literature

2.1. Reversible addition-fragmentation chain transfer polymerization

Reversible addition-fragmentation chain transfer polymerization (RAFT) has attracted attention in recent years due of the urgent need of controlled polymerization techniques for synthesis of well-defined block copolymers. This reversible deactivation radical polymerization (RDRP) is considered as the most versatile one among other RDRPs. RAFT shows great compatibility with wide range of monomers and reaction media. Degenerative chain transfer is based on use of thiocarbonylthio compounds as chain transfer agents, that are transported along the growing polymer chain.[1,2] General mechanism of RAFT polymerization (Figure 1) consists of creating propagating radical formed by reaction of monomer and initiating radical. This propagating radical is added to C=S group of RAFT agent, this process creates an intermediate radical. Fragmentation of this intermediate creates new radical and polymeric thiocarbonylthio compound. Newly formed radical is able to reinitiate monomer polymerization and a new propagating radical is created. Active propagating radicals are together with polymeric thiocarbonylthio compound in equilibrium state. This step is essential to chain growth. Thiocarbonythio end-group remains attached to the polymer chain. Last step is termination of active radicals.[3]

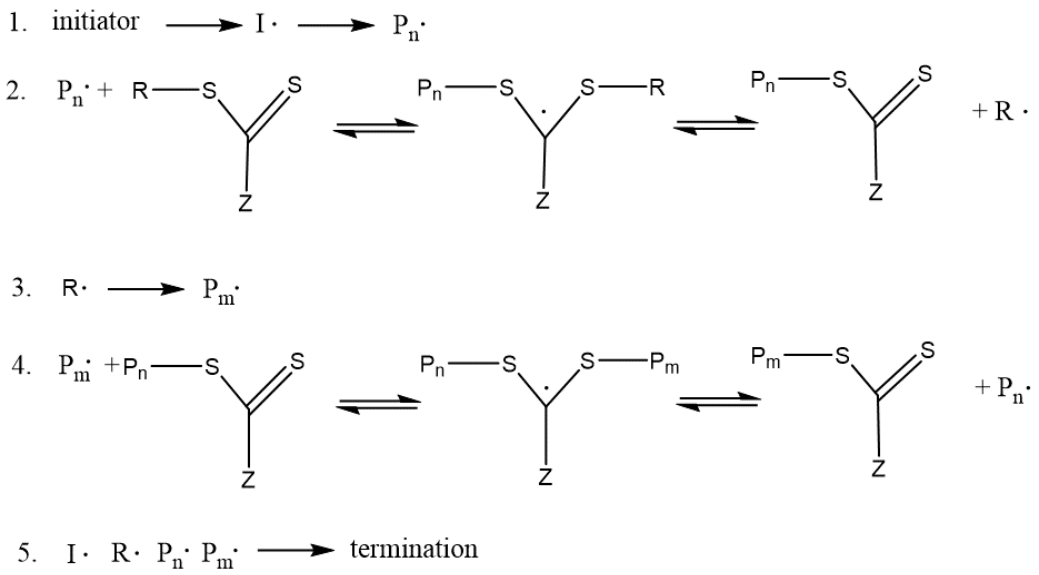

Figure 1: Simplified scheme od RAFT polymerization mechanism.[1]

Designing the RAFT agent is an important step in RAFT polymerization. Temperature and monomer type must be taken into consideration because of their influence of the kinetics and thermodynamics of polymerization process. Different properties can be achieved by changing Z and R group of RAFT agent (shown in Figure 1). Other types of agents are macromolecular RAFT agents (macroRAFT) that function both as control agent and stabilizer.[4]

2.2. Block copolymer architecture

Block copolymers are polymers composed of two or more various monomeric units (segments) forming distinct polymer blocks, which can be arranged into linear, branched and cyclic molecular architectures. According to their sequential arrangement block copolymer structures range from simple diblock A-B structures to triblock or multiblock structures with many distinct segments.[5] Properties such as chemical resistance, thermal properties or solution behaviour are influenced by segments in polymer and can be regulated by changes in those segments. In amphiphilic diblock copolymers (A-B), the polymer blocks are both solvophilic (block A) and solvophobic (block B). Such copolymers thus resemble head-and-tail structure of conventional low molecular weight surfactant.[5,6]

2.3. Self-assembly of amphiphilic diblock copolymers in aqueous solutions

Factors that influence the nanostructures obtained by self-assembly of AB diblock copolymers are temperature, the properties of individual blocks, their compatibility with each other and solvent composition. Important factor in obtaining self-assembly structures is selection of a solvent.[7] The selectivity refers to fact that a certain solvent is good solvent for one block and poor solvent or non-solvent for other block of a copolymer. Micelle formation occurs above a specific equilibrium concentration, called the critical micelle concentration (CMC). Block copolymers can self-assemble into micelles with core-shell structures in selective solvents above the CMC. Morphologies, such as spheres, worms or rods are also commonly observed. The micelle core is formed by the insoluble, hydrophobic block, which is trying to avoid contact with solvent, in this case water, and the corona is formed by soluble hydrophilic block.[7,8]

2.4. Coassembly of diblock copolymers

Coassembly is an important property of polymers and nanoparticles, that enables us to create new hybrid nanostructures with complementary characteristics combining both inorganic and organic properties. As a term coassembly is the most often used for interaction of polymers (polyelectrolytes) with low molecular weight agents (ions). Nanostructures can also form by interaction of positively charged polymers and nonclassical anions.[9]

Anionic boron cluster compounds (ABCCs) belong to previously mentioned non classical anions that are able to form complexes with polymers or proteins through weak interactions.[10] Charge density plays an important role in ABCCs chemical reactions. A two-electron three center bond, with delocalized electrons over the cluster, gives these compounds their atypical shape and aromatic character. Common boron compounds used in polymer science are *closo*-boranes ($[B_nH_n]^{2-}$), carboranes, where one or more carbon atoms are incorporated to cluster and metallacarboranes (Figure 2). These boron clusters show amphiphilic behaviour and are involved in dihydrogen bonging with proteins, polymers and other nanostructures.[10,11]

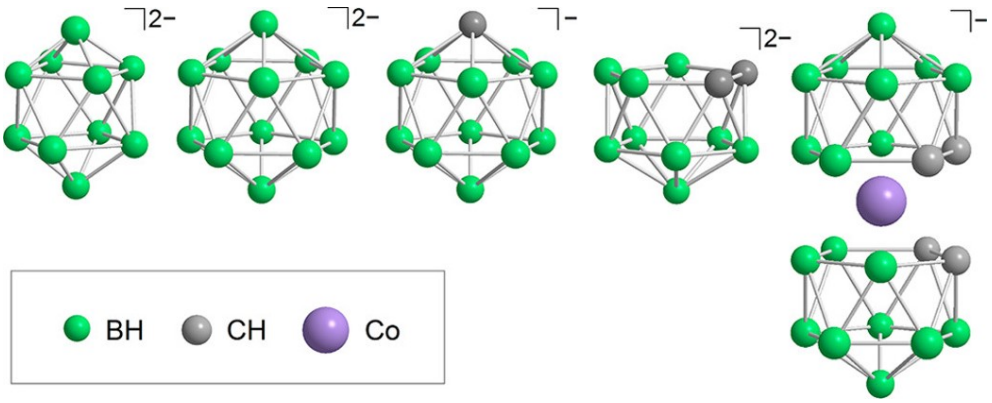

Figure 2: Typical examples of anionic boron cluster compounds (left to right): decaborate $[B_{10}H_{10}]^{2-}$; dodecaborate $[B_{12}H_{12}]^{2-}$; 1-carbadodecaborate $[CB_{11}H_{10}]^{-}$; 1,2-dicarbollide $[1,2\text{-}C_2B_9H_{11}]^{-}$; COSAN $\{3,3'\text{-}Co[1,2\text{-}C_2B_9H_{11}]_2\}^{-}$.[10]

Another interesting ion that can induce a coassembly of diblock copolymer is guanidinium cation. Guanidium is a flat triangular molecule that has hydrophobic centre and hydrophilic sides. Furthermore, thanks to π-π interaction the stacking of guanidinium ions is possible.[10-12] Arginine-rich proteins contain guanidinium on a side

chain is able to penetrate cell membrane. Therefore, functionalized polymer containing guanidinium groups can influence cell permeability and cellular uptake.[13]

2.5. Techniques for micelle-structure characterization

Micelles can be assembled to various morphologies and their structure can be characterized by variety of scattering, spectral and separation techniques. Primarily, to determine the structure of polymer, nuclear magnetic resonance is often used. Thanks to different scattering methods like light scattering, Small Angle X-ray scattering (SAXS) we are able to determine nanoparticle size distribution, size and shape of micelles and other properties such as aggregation number, which is the number of copolymers chains forming a micelle. In recent years, to characterize the structure of nanoparticles in solution cryogenic transmission electron microscopy (cryo-TEM) has been used.

2.5.1. Light scattering

The electric field of a light wave acting on a particle induces in it a dipole that oscillates with the same frequency as the incident light. An oscillating dipole produces a secondary oscillating field. This field radiates electromagnetic energy and this particle, a scatterer, scatters the incident light. For macroscopic system, the overall scattering is caused by interference effect of all scattering components. Intensity of a scattered light depends on a wavelength of a light (λ), it increases with the inverse fourth power of the wavelength.[14,15] In case of liquids, the scattering is caused by density fluctuations. For colloids, dispersions of nanoparticles and solutions of macromolecules, the scattering is caused by concentration fluctuations and the spatial distribution of the scattered light, which reflexes the size and shape of nanoparticle. In light scattering measurements, an important parameter is scattering angle (θ), which characterizes the angle in which a particle deflects a light beam when it comes in contact with it. The two basic approaches of the light scattering measurement are: dynamic and static light scattering. [14,16,17]

The static light scattering (SLS) is method based on the fact that when light passes through a solution some portion of the light will be scattered in all directions. Measured is average intensity of the scattered light as a function of the scattering angle θ.

The scattering vector $\vec{q}$ is quantity defined by the difference of the wave vectors of the scattered light $\vec{k}$ and the incident light $\overrightarrow{k_0}$

$$\vec{q} = \vec{k} - \overrightarrow{k_0} \tag{1}$$

For SLS, $q = 2a$ where $a = k \cdot \sin\frac{\theta}{2}$ and $k = \frac{2\pi}{\lambda}$. If λ is substituted by the relation of the wavelength of the incident light and the refractive index of the medium, $\frac{\lambda_0}{n}$, we get amplitude of the scattering vector expressed as

$$q = \frac{4\pi n}{\lambda}\sin\frac{\theta}{2} \tag{2}$$

The Zimm equation

$$\frac{Kc}{R} = \frac{1}{M_{\mathrm{W}}P(q)} + 2A_2c + \cdots \tag{3}$$

shows relation between the scattered intensity, concentration and the amplitude of the $\vec{q}$, where $R(q,c)$ is a normalized scattered intensity (Rayleigh ratio), A_2 is a second virial coefficient that describes attractive and repulsive forces between particles and K is the constant dependent on refractive index increment as follows

$$K_C = \frac{4\pi^2 n_0^2 \left(\frac{\mathrm{d}n}{\mathrm{d}c}\right)^2}{\lambda^4 N_{\mathrm{A}}} \tag{4}$$

where N_{A} is Avogadro constant and $\frac{\mathrm{d}n}{\mathrm{d}c}$ is refractive index increment of the sample concerning the solvent. Refractive index increment $\frac{\mathrm{d}n}{\mathrm{d}c}$ of a solution characterizes the changes of refractive index with a solute (polymer) concentration. It is an essential parameter for determination of the average molecular weight M_{W}. If the dependence of $\frac{K_C}{R}$ on q is extrapolated to $\theta = 0°$ and concentration $c = 0$ g/L, the intercept is equal to $1/M_{\mathrm{W}}$. The q-dependent term $P(q)$ is a form factor, which is equal to 1 if the particles are smaller than $\frac{\lambda}{20}$. For larger particles of any shape in so called Guinier region, the form factor can be expressed as function of radius of gyration, R_{G}, as follows

$$P(q) = 1 - {}^1\!/_3\, R_{\mathrm{G}}^2 q^2. \tag{5}$$

The Zimm equation is usually graphically expressed as Zimm plot (Figure 3), which enables determination of the gyration radius R_G weight-averaged molar mass of nanoparticles M_W, and second virial coefficient A_2. For obtaining the aggregation number, N_{agg}, the molar mass of the nanoparticle is divided by M_W of the micelle forming polymer chains.

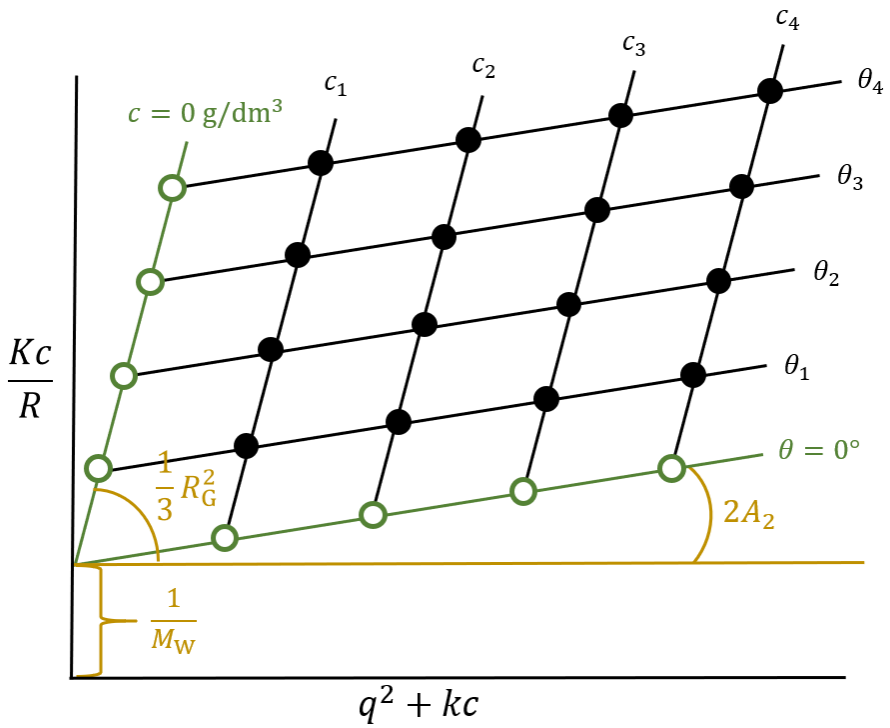

Figure 3: Model Zimm plot-extrapolation of scattering intensity to zero angle, θ, and zero concentration, c, where M_W is absolute molecular mass, R_G is radius of gyration and A_2 is second virial coefficient.

In the dynamic light scattering (DLS) we assume that the scattering particles are present in a solution free to move around by Brownian motion. The light beam is being attenuated when it passes through a solution. Either absorption or scattering (or both) weakens the intensity of the light beam. DSL disregards the intensity of the scattered light but uses the temporal fluctuations in the scattered light. In conclusion the information about the size and diffusion coefficient of the molecule comes from fluctuation times for the scattered intensity.[14, 15]

In DLS experiment an intensity correlation function $G_2(\tau)$ is measured and can be expressed as

$$G_2(\tau) = \langle I(t)I(t+\tau)\rangle \tag{6}$$

where τ is lag time between two time points and (t + τ) is delayed time. This intensity correlation unction can be normalised and determined as

$$g_2(\tau) = \frac{\langle I(t)I(t+\tau)\rangle}{\langle I(t)\rangle^2}. \tag{7}$$

The DLS data can be analysed by two methods. First, cumulant method is usually based on assumption that the system is monomodal, meaning that the particle size distribution is Gaussian.[16, 18] To obtain the diffusion coefficient (z-average), D_Z, from logarithm of the autocorrelation function a polynomial fit has to be implemented, which gives us the decay rate Γ (1. cumulant), that is related to diffusion coefficient D

$$\Gamma = q^2 D. \tag{8}$$

Diffusion and size of the spherical particle is expressed in Stokes-Einstein equation:

$$D = \frac{k_B \cdot T}{6\pi\eta r} \tag{9}$$

where T is the absolute temperature of the suspension, η is dynamic viscosity and k_B is the Boltzmann´s constant and r is the radius of the spherical particle. Particles that are moving quickly (bigger diffusion coefficient) are smaller in size and correspond to the rapidly fluctuating scattered intensity. Radius of hypothetical sphere that has the same diffusion as experimentally found value D_{exp} by using the Stokes-Einstein equation it defines so called hydrodynamic radius R_H, which can also include the hydration shell of the micelle[16,17]

$$R_H = \frac{k_B \cdot T}{6\pi\eta D_{exp}}. \tag{10}$$

The experimentally obtained values of diffusion coefficients are apparent, and to obtain the true value of D_z, the apparent values have to be extrapolated to θ = 0° and concentration c = 0 g/L, that is usually expressed as dynamic Zimm plot.

On the other hand, the CONTIN method is more suitable for polydisperse systems. The CONTIN method involved inverse Laplace transformation, which provides a distribution of correlation times, which can be recalculated by using Stokes-Einstein equation to distribution of hydrodynamic radii.[18]

An estimation of the particle shape is provided by shape factor of particles expressed as R_G/R_H. When taking into account R_H and R_G values the shape of nanoparticles can vary between spheres, oblate ellipsoids through worms or rods.[16,17]

2.5.2. Nuclear magnetic resonance

Nuclear magnetic resonance (NMR) is spectroscopic method used in polymer chemistry not only for the chemical structure determination but also for determination of polymer stereoisomerism (so called tacticity) or for number-averaged molecular weight characterization.[19] The most important characteristic involved in NMR is the nuclear spin, $\vec{I}$. NMR experiments can only be conducted with nuclei with non-zero nuclear spin. Examples of nuclei with $\vec{I} = 0$, meaning they have no magnetic moment, are ^{12}C, ^{16}O, ^{32}S where number of both protons and neutrons is even. On the other hand, when the combined number of protons and neutrons is odd, $\vec{I}$ gains half-integer values (1/2, 3/2, 5/2). In case if both number of protons and number of neutrons is odd, $\vec{I}$ gains integer values (1, 2, 3). Nuclei with half-integer or integer nuclear spin have magnetic dipole moment, $\vec{\mu}$, which is related to $\vec{I}$ via following relation

$$\vec{\mu} = \gamma \cdot \vec{I} \tag{11}$$

where γ is gyromagnetic ratio, that is defined as

$$\gamma = \frac{g_N \mu_N}{\hbar} \tag{12}$$

where ħ is reduced Planck constant, g_N is the g-factor and μ_N is the nuclear magneton.[19] When magnetic field is applied to nuclei with non-zero magnetic spin, nuclear energy levels are split according to their magnetic quantum number m. For most commonly observed nuclei like ^1H, ^{13}C, ^{31}P with $\vec{I}$ = ½, have two magnetic states m = ½ and m = −½. In magnetic field, B_0, magnetic moment is can be aligned to B_0 in parallel manner (m = ½) or in antiparallel manner (m = −½).[20] In these two directions the spins are not distributed

equally and therefore the nucleus has a magnetic dipole moment with energy in magnetic field defined as

$$E = -\vec{\mu} \cdot \overrightarrow{B_0}. \tag{13}$$

The frequency of the electromagnetic radiation that induces a transition from one spin to another also called Larmor frequency depends on both nuclear magnetic moment and magnetic field. External magnetic field induces motion of electrons. These electrons cause effect called nuclear shielding, σ, by generating secondary magnetic fields and therefore the effective magnetic field, B_{eff}, is decreased. For observed nuclei, the resonance frequencies are influenced by local environment, these detected frequencies are referred to as chemical shifts, δ. The chemical shift is given in parts per million (ppm) and is defined as

$$\delta = \frac{\omega - \omega_{ref}}{\omega_{ref}} \tag{14}$$

where ω is frequency of interest and ω_{ref} is frequency of a reference, which is signal from a standard molecule. For the atoms of the same type, that are chemically equivalent, their resonance frequencies are identical. Recognising equivalency of atoms within the same molecule and knowledge of the chemical shifts of functional groups are key factors in interpreting NMR spectra.[19,20]

2.6. Applications of polymer micelles

In recent years, polymeric micelles have been studied as a possible option for nanocarrier in drug delivery or radiotherapy. Micelles with copolymers as building block showed favourable properties for medical use such as biocompatibility, ability to target afflicted tissue and accumulate there or stability *in vitro* and *in vivo*. Polymeric micelles are studied as potential boron delivery agents, where selective tumor targeting is still a challenging task. [Attachment A]

2.6.1. Drug delivery

Particularly appealing for drug delivery applications are linear copolymers. By using controlled polymerization techniques these polymers benefit from the properties of two or more monomers in a single polymer chain. These copolymers are commonly prepared

by RAFT polymerization which allows to control their properties such as polymer length or overall distribution of monomers. Recently, guanidinium-rich copolymers were used in drug delivery.[21] Thanks to amphiphilic properties of guanidinium arginine-rich proteins are able to penetrate cell membrane. That led to exploration of properties of copolymers containing guanidinium. Therefore, these polymers are studied as drug delivery systems together with *closo*-dodecaborate anion, which was chosen because of its high boron content. Shape of the nanoparticles is also influential to intracellular transport and uptake.[21, 22]

A controlled release of the drug delivery system into tumor is still subject of research. Many controlled release technologies were developed over the years, including diffusion-controlled matrices methods, chemically regulated biocompatible materials or solvent-activated hydrogels. More recently materials have been introduced that respond to environment conditions.[23]

2.6.2. Boron neutron capture therapy

One of the essential methods in cancer treatment is radiotherapy. Boron neutron capture therapy (BNCT) is selective form of radiotherapy.[24] The first step of the procedure is localization of a cancerous cell. This is achieved by delivery system containing non-radioactive isotope of boron (^{10}B) of a certain concentration. However, the desired concentration of boron-10 in tumor is relatively high (at least 30μg ^{10}B per gram of tumor) and delivery through blood-brain barrier is also problematic due to poor permeability. Recently, nanoparticles had an important role as delivery systems. Boron-10 is then irradiated with neutron source, this causes neutron capture reaction where boron-10 absorbs neutrons and produces the α particle (^{4}He) and lithium nucleus (^{7}Li). The lethality of these two particles formed by this neutron capture for tumor cells is a key factor together with ability to target cancerous cells and distinguishing them from healthy tissue.[24,25]

3. Aims of the thesis

This thesis is a contribution to the long term study of boron-rich nanoparticles formed by block copolymers and boron cluster compounds in the Soft Matter research group, Department of Physical and Macromolecular Chemistry. The aims of this bachelor thesis are following:

1. To prepare stable nanoparticles (micelles) by using poly(2-vinyl pyridine)-*b*-poly(ethylene oxide) and poly(ethylene oxide)-*b*-poly(2-(N, N, N′, N′-tetramethyl guanidinium) ethyl acrylate) by coassembly with sodium *closo*-dodecaborate.

2. To characterize the prepared micelles by static and dynamic light scattering and NMR spectroscopy methods.

3. To study impact of ionic strength on the prepared micelles in terms of size and molar mass in two types of aqueous solutions: pure water and 0.156M NaCl (physiological solution).

The obtained knowledge will allow for a reproducible preparation of stable boron-rich nanoparticles and further studies of coassembly process of block copolymers as well as their possible use as drug delivery and boron delivery agents.

4. Materials and used methods

4.1. Used polymers and other reagents

Poly(2-vinyl pyridine)-*b*-poly(ethylene oxide), $P2VP_{129}$-*b*-PEO_{477}, was purchased from Polymer Source, Inc. (Dorval, Quebec, Canada). The structure is shown in Figure 4 (right). This polymer was synthesized by living anionic polymerization with resulting dispersity $Đ$ = 1.1. The weight-averaged relative molecular weight of the P2VP and PEO blocks, provided by the manufacturer, are 13.5×10^3 and 21.0×10^3, respectively. Further information on the synthesis and sample characterization can be found on webpages of the supplier Polymer Source under sample #P2492-2VPEO.

Poly(ethylene oxide)-*b*-poly(2-(N, N, N′, N′-tetramethyl guanidinium) ethyl acrylate), PEO_{114}-*b*-$PGEA_{23}$, block copolymer was synthesized by Jianwei Li (Ph.D-student in Soft Matter research group) by RAFT polymerization (brief summary of synthesis is in the section 5.1.). [Attachment A] The structure is shown in Figure 4 (left) and M_n = 12,156, $Đ$ = 1.18. [Attachment A]

Materials used for PEO-b-PGEA synthesis: 2-bromoethanol (95%), acryloyl chloride (97%, contains <400 ppm phenothiazine as stabilizer), triethylamine (TEA, ≥99.5%), 1,1,3,3-Tetramethylguanidine (99%), methoxy poly(ethylene oxide) (mPEO) with different molecular weights (around 2, 5, 10 kDa) were purchased from Sigma-Aldrich. All other reagents were purchased from commercial sources and used as received.

Sodium *closo*-dodecaborate (anhydrous), $Na_2[B_{12}H_{12}]$, was purchased from KatChem Ltd., Czech Republic, and used without further purification.

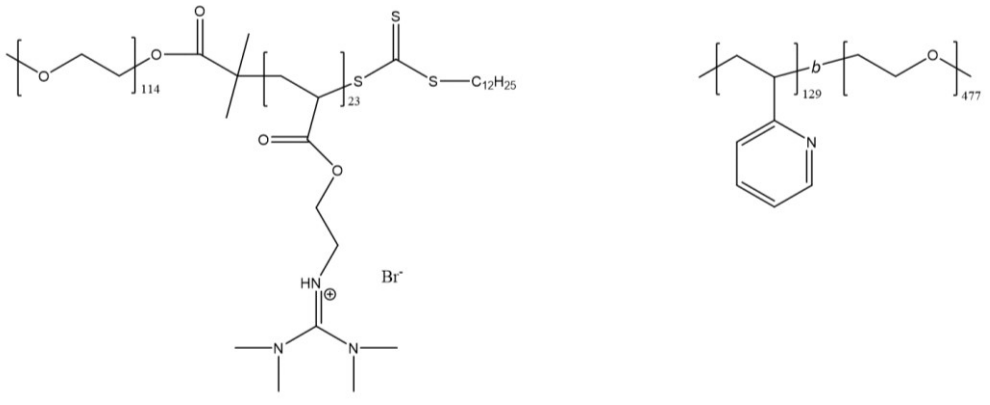

Figure 4: Structures of used polymers: on left PEO_{114}-b-$PGEA_{23}$, on right $P2VP_{129}$-b-PEO_{477}.

4.2. Micelles preparation

The micelles of PEO_{114}-*b*-$PGEA_{23}$ with $Na_2[B_{12}H_{12}]$ were prepared as follows.

Two types of experiments were carried out. In the first one, 2 mg of polymer was dissolved in 2 mL of both pure water and 0.156 M NaCl solution, so the concentration of polymer would be 1 g/L. The 0.156 M NaCl solution has been chosen as solvent because of biological relevance. Polymer sample was filtrated. Beforehand 0.1 M solution of sodium dodecaborate has been prepared and this solution has also been filtrated. Dodecaborate solution was added to polymer sample to obtain dodecaborate/guanidine ratios 0.00, 0.05, 0.10, 0.15, 0.20, 0.25, 0.30, 0.35, 0.40, 0.50, 0.60, 0.80, 1.00, and 1.50. After each addition light scattering measurement has been performed. This technique can be termed as "titration experiment", and this type of experiment was carried out also for NMR spectroscopy analysis.

For the second type of experiment, so called "Zimm plot experiment", 20 mg of polymer was dissolved in 10 mL in both pure water and in 0.156 M NaCl (concentration of polymer was 2 g/L). Polymer sample was filtrated. New 0.1 M solution of sodium dodecaborate has been prepared, filtrated and added to polymer sample, so the ratio of dodecaborate/guanidine would be 0.5. Finale mixtures serve as stock solutions for light scattering analysis. Samples for both static and dynamic Zimm plots were prepared from stock solutions and they were diluted to gain five samples with concentrations of polymer 0.25 g/L, 0.50 g/L, 1.00 g/L, 1.50 g/L and 2.00 g/L, again for both pure water and for 0.156 M NaCl solution. The overall micelle concentrations were recalculated due to the dodecaborate addition to diblock copolymer solutions (weight fraction of dodecaborate is around 9.4 w-% assuming the quantitative binding of dodecaborate to the micelles) [Attachment A] as follows: 0.265 g/L, 0.530 g/L, 1.06 g/L, 1.59 g/L, and 2.12 g/L. From the stock solutions in water and 0.156 M NaCl, samples with volume 10 mL for refractive index increment measurement were prepared. Stock solutions were diluted to get the sample (copolymer with dodecaborate) concentrations 0.085 g/L, 0.106 g/L, 0.212 g/L, and 0.318 g/L.

The micelles of $P2VP_{129}$-PEO_{477} with $Na_2[B_{12}H_{12}]$ in acidic solutions were prepared by following procedure using "titration experiment" for NMR spectroscopy testing. Due to the low stability of $P2VP_{129}$-PEO_{477}/$[B_{12}H_{12}]$ solutions that are prone to precipitation no

detailed light scattering testing was carried out. In vial, 20 mg of polymer was dissolved in solvent prepared by mixing 53 μL of DCl and 1947 μL of D_2O. pH of solution was 0.48. Subsequently, 3 M solution of sodium dodecaborate was prepared by dissolving 11.2 mg in 20 μL of D_2O. Dodecaborate solution was added to polymer sample to obtain dodecaborate/2-vinyl pyridine ratios 0.00, 0.15, 0.30, 0.50, 0.80 and 1.00. As standard 0.2 μL of *t*-butanol (*t*-BuOH) was added. After each addition ^{1}H NMR spectrum has been measured.

4.3. Refractive increment index

The values of refractive index increment, d*n*/d*c*, for determination of the absolute micellar M_W for PEO_{114}-*b*-$PGEA_{23}$/$[B_{12}H_{12}]$ samples in both pure water and 0.156 M NaCl, $(dn/dc)_{water}$ and $(dn/dc)_{salt}$, respectively, were measured by the Optilab T-rEX refractive index detector, Wyatt Technology Corporation. During the experiment, the solvent (water or 0.156 M NaCl) and the micelle samples with volumes of 10 mL (concentrations 0.085 g/L, 0.106 g/L, 0.212 g/L, and 0.318 g/L) were consecutively injected by the mechanical pump equipped with plastic syringe and membrane filter into the detector with the flow rate 1 mL/min. Then, the relative refractive index change with time was recorded for samples in water and 0.156 M NaCl. The heights of plateaus corresponding to individual sample concentrations in respect to the solvent were plotted against the sample concentrations, and the values of (d*n*/d*c*) were obtained by a linear fit.

4.4. Static and dynamic light scattering

The light scattering measurements (SLS and DLS) were performed on photometer (ALV, Germany) consisted of CGS-3 automatic goniometer, a 7004 multitau multibit autocorrelator, two high-QE APD pseudo cross-correlation detectors, and a 100 mW, 660 nm diode-pumped solid-state laser. Both static and dynamic light scattering were performed at 23 °C for the scattering angles ranging from 30° to 150°, with an angular step of 10°. DLS data analysis was performed by fitting the measured normalized intensity autocorrelation function $g_2(t) = 1 + \beta|g_1(t)|^2$, where $g_1(t)$ is the electric field correlation function, t is the lag time and β is a factor accounting for deviation from the ideal correlation. DLS analysis by CONTIN method provides the distribution of relaxation times, $\tau A(\tau)$. Effective angle and concentration-dependant hydrodynamic radii, $R_H(q,c)$, were

obtained from the mean values of relaxation times, $\tau_m(q,c)$, of individual diffusive modes using the Stokes-Einstein equation. To obtain true hydrodynamic radii, the values of D_{exp} have to be extrapolated to a zero scattering angle. The SLS data were treated by standard Zimm method.

4.5. Nuclear magnetic resonance

NMR spectra for block copolymer PEO_{114}-*b*-$PGEA_{23}$ were measured by Jianwei Li. ^1H NMR spectra were measured on a Varian ^{UNITY}*INOVA* 400 in $CDCl_3$ and deuterium oxide (99.5 %; Chemotrade, Leipzig, Germany). Spectra were referenced to the solvent signal (4.80 ppm).

NMR spectra for block copolymer $P2VP_{129}$-*b*-PEO_{477} were measured with help of PhD-student Roberto Fernandez-Alvarez on a Varian ^{UNITY}*INOVA* 300 in DCl and deuterium oxide (99.5 %; Chemotrade, Leipzig, Germany).

4.6. Cryo-TEM

The Cryo-TEM measurements were performed by Dr. Sami Kereïche from Institute of Cellular Biology and Pathology, First Faculty of Medicine, Charles University, Prague. [Attachment A] For Cryo-TEM measurement a 3 μL drop of the sample solution was applied to an electron microscopy grid with carbon-covered polymer supporting film (lacey-carbon grids LC200-Cu, Micro to nano, NL), glow discharged for 30 s with 5 mA current. Most of the sample was removed by blotting (Whatman No. 1 Filter paper) for 1 s, and the grid was immediately plunged into liquid ethane held at −183 °C. The sample was then transferred without rewarming into a TecnaiSphera G20 electron microscope (FEI, Hillsboro, OR) using a Gatan 626 cryo-specimen holder (Gatan Inc., Pleasanton, CA). Images were recorded at 120 kV accelerating voltage and microscope magnifications ranging from 5000× to 14500× using a GatanUltrScan 1000 slow scan CCD camera (giving a final pixel size from 2 to 0.7 nm). The applied under-focus typically ranged between 1.5 and 2.7 microm. The applied blotting conditions resulted in the specimen thickness varying between 100 and 300 nm.

5. Results and discussion

5.1. Synthesis of PEO_{114}-b-$PGEA_{23}$

The poly(ethylene oxide)-*block*-poly(2-(N, N, N′, N′-tetramethyl guanidinium) ethyl acrylate), PEO_n-*block*-$PGEA_m$, block copolymers were prepared by Jianwei Li. [Attachment A] These copolymers of various length were prepared by RATF polymerization. In first step a RAFT agent S-1-Dodecyl-S′-(R,R′-dimethyl-R″-acetic acid) trithiocarbonate (TTCA) was prepared. In the next step a monomer 2-bromethyl acrylate (BEA) was synthesized by using 2-bromethanol, triethylamine and acryloyl chloride as reactants. An organic phase containing monomer was dried, removed by rotary evaporation and product was purified by distillation. In following step TTCA was dissolved in dichloromethane (DCM) and to this solution oxalyl chloride was added. Later PEO_{45} in DCM was added to reaction mixture. The PEO-TTCA was precipitated in cold diethyl ether, separated by centrifugation and further purified in THF and cold diethyl ether. In this step, the hydroxyl end group of the PEO was functionalized using RAFT agent. The synthesis continued by RAFT polymerization of PEO-*b*-PBEA block copolymer. In summary, to a PEO-*b*-TTCA solution BEA was added, followed by three freeze-pump-thaw cycles. The three freeze-pump-thaw cycle were also carried on AIBN solution. Both solutions were mixed and stirred, the products were precipitated in cold diethyl ether. To synthesize PEO-*b*-PGEA, polymer from previous step was dissolved in DMF and 1,1,3,3-Tetramethylguanidine was added. The mixture was stirred overnight and final product was precipitated in cold diethyl ether and separated by centrifugation. Analogically were prepared block copolymers with different length of PEO and PGEA blocks. For all the copolymers the degree of polymer was decided by ^{1}HNMR spectroscopy.[26, 27]

The sample PEO_{114}-*b*-$PGEA_{23}$ has been selected for the experiments carried out in this Thesis.

5.2. *Micelle characterization*

5.2.1. *Static and dynamic light scattering*

Only PEO_{114}-*b*-$PGEA_{23}$ diblock copolymer samples were characterized by light scattering and cryo-TEM techniques, because $P2VP_{129}$-*b*-PEO_{477} samples were unstable and were prone to precipitation after the dodecaborate addition.

0.1 M solution of sodium dodecaborate was added to PEO_{114}-*b*-$PGEA_{23}$ block copolymer solution with concentration 1 g/L in water and in 0.156 M NaCl, to achieve the dodecaborate/guanidine ratios 0.00, 0.05, 0.10, 0.15, 0.20, 0.25, 0.30, 0.35, 0.40, 0.50, 0.60, 0.80, 1.00, and 1.50. For all the ratios angle-dependent LS-intensity was measured, and its extrapolation to a zero scattering angle is displayed in Figure 5.

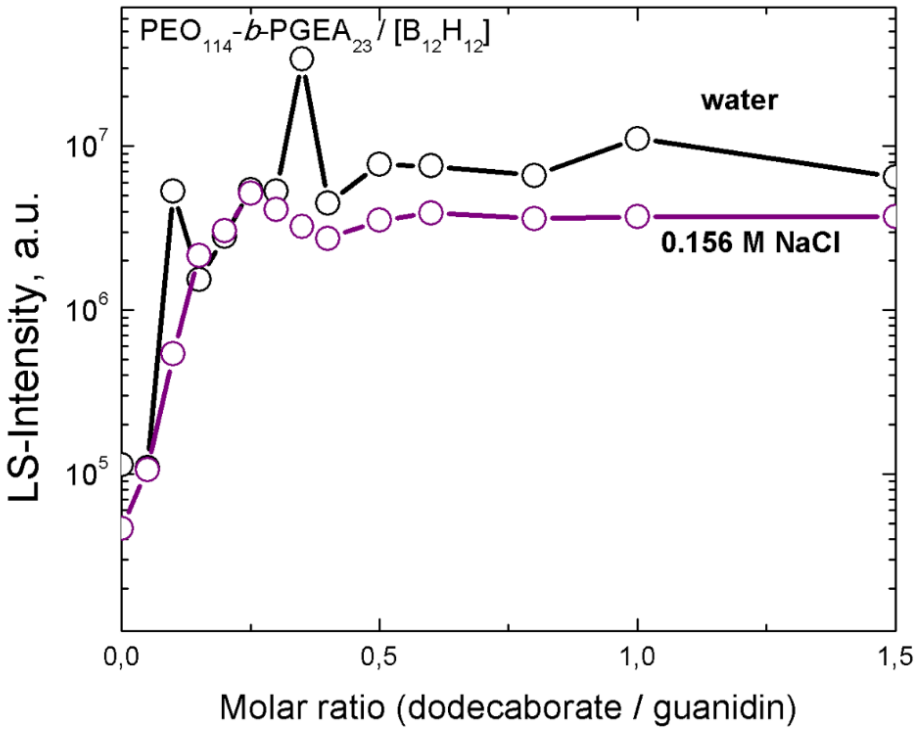

Figure 5: Light scattering intensity extrapolated to a zero scattering angle after sodium dodecaborate addition to PEO_{114}-b-$PGEA_{23}$ in water and in 0.156M NaCl solution.

After the addition of dodecaborate to diblock copolymer solutions in both pure water and salt solution we can see almost immediate increase of the relative LS-intensity, which is proportional to molar mass of the scatterers. It increased by around two orders of

magnitude. In the region of dodecaborate/guanidine ratios 0.25-0.50, the LS-intensity levels-off. By DLS analysis (not shown; details in [Attachment A]), we observed the same trend as for SLS data in Figure 5. All samples are mostly monomodal with initial hydrodynamic radius, R_H, around 4 nm (pure polymer with no dodecaborate) that increased to around 13 nm for the copolymer dodecaborate mixtures. This major mode was accompanied with small fraction of undefined particles with radius around 250-500 nm (dust and micellar aggregates, which were omitted from the evaluation).

Both SLS and DLS indicated that pure PEO_{114}-*b*-$PGEA_{23}$ is molecularly soluble in water and NaCl solution and formed stable uniform nanoparticles after the addition of dodecaborate anions. With further addition of dodecaborate molar mass of the nanoparticles (their aggregation number) does not change for the ratios above 0.5, and we can deduce that at this point micelles are already saturated by dodecaborate.

To obtain the absolute values of the micellar M_W and the aggregation number from static light scattering measurements for boron-rich nanoparticles, it requires the values of refractive index increment $\frac{dn}{dc}$ that was measured for nanoparticles in water and in 0.156 M NaCl solution. Diluted micellar samples were consecutively injected to the refractometer starting with pure solvent (further details in the section 4.3). The raw data are shown in Figure 6 (left), the first flat line of the curve represents solvent. Every step represents individual concentration beginning with the lowest one. Little peaks and fluctuations were caused by the syringe changes. From flat lines representing each concentration the values of Δn has been taken and plotted against the micelle concentration (Figure 6-right). Refractive index increment is the slope of linear fit. Measured values of $\frac{dn}{dc}$ for nanoparticles for water and for 0.156M NaCl are $\frac{dn}{dc}_{water} = 0.207\ \mathrm{mL/g}$ and $\frac{dn}{dc}_{salt} = 0.230\ \mathrm{mL/g}$, respectively. Both values are almost the same within the experimental error. Because the concentration of the stock NaCl solution used for the refractive index experiment slightly differed from the salt concentration in the micelle samples, the value of Δn for pure solvent was adjusted in a way to be exactly 0, which ensured the linearity of all values used for the refractive index increment evaluation.

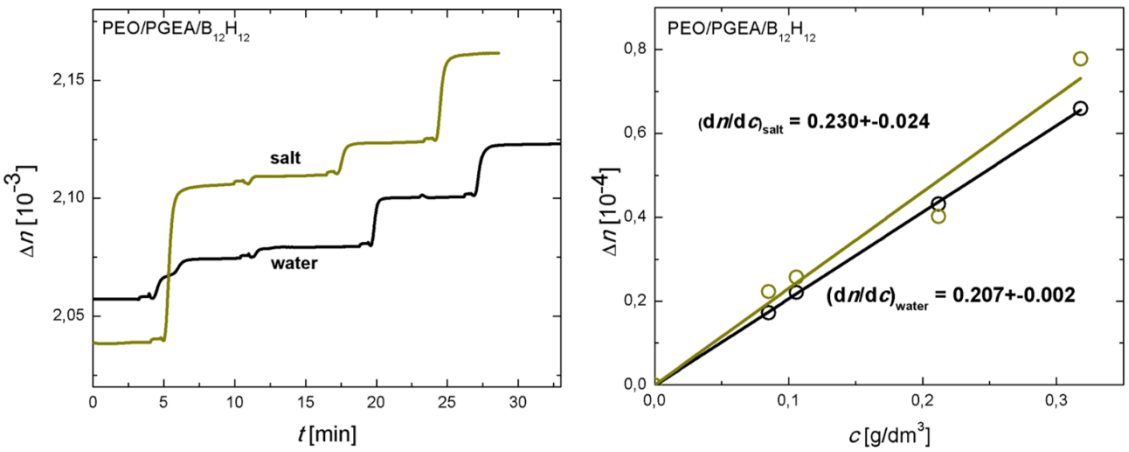

Figure 6: Raw data from the refractive index measurement (left); obtained Δn values plotted against micelle concentration were further treated by a linear fitting and the values of the refractive index increment were evaluated (right).

The PEO_{114}-*b*-$PGEA_{23}$/$[B_{12}H_{12}]$ samples with polymer concentrations 0.25, 0.50, 1.00, 1.50 and 2.00 g/L and the dodecaborate/guanidinium ratio 0.5 in pure water and in 0.156 M NaCl solution were prepared and "Zimm plot experiment" was carried out (further details in the sections 4.2 and 4.3), the resulting Zimm plots are presented in Figure 7.

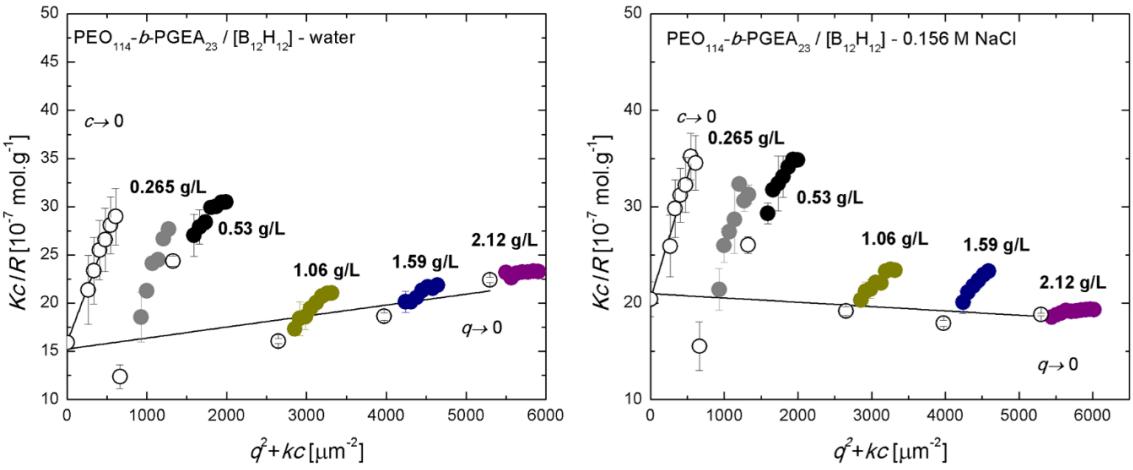

Figure 7: Zimm plots of PEO_{114}-b-$PGEA_{23}$/$[B_{12}H_{12}]$ in pure water and in 0.156M NaCl solution.

The Zimm plots enabled evaluation of the weight-averaged micellar molar mass, M_W, the micellar aggregation number, N_{agg}, and the values of the radius of gyration, R_G, the second

virial coefficient, A_2 in water and salt solution. The results are summarized in Table 1.

Table 1: Evaluation of static Zimm plots of PEO_{114}-b-$PGEA_{23}$/[$B_{12}H_{12}$] micelles in water and 0.156 M NaCl solution, where R_G is radius of gyration, M_W is weight averaged molecular mass, A_2 is second virial coefficient and N_{agg} is aggregation number. The molar mass of diblock copolymer used for the calculation of N_{agg} was 12.156 g/mol.

Sample	M_W **[10^5 g/mol]**	A_2 **[10^{-7} mol·L/g^2]**	R_G **[nm]**	N_{agg}
PEO-PGEA/B12 - water	6.279 ± 1.720	1.281 ± 1.678	64.55 ± 2.58	47 ± 13
PEO-PGEA/B12 - salt	4.898 ± 0.920	−0.410 ± 1.476	60.85 ± 5.56	37 ± 7

The absolute weight averaged molecular mass, M_W, of coassembled nanoparticles is lower in 0.156 M NaCl solution than in pure water. Considering that dodecaborate anions are quantitatively incorporated into the micelles in both water and salt solution with the same dodecaborate weight fraction (up to) 9.6 w-%, it means that number of polymeric chains forming one micelle is also lower in salt solution. Micelles show excellent stability in both water and in salt solution, and no CMC has been detected. We can presume that specific weak interaction and electrostatic attraction between positively charged guanidine and dodecaborate contribute to a coassembly process. [Attachment A] Additional experiments [Attachment A] also suggest that the loading capacity and the binding constant of dodecaborate in the micelles considerably changes with ionic strength, and that the dodecaborate fractions in salt solution is close to 9.6 w-%, while it can be lower in pure water. [Attachment A]

Second virial coefficient, A_2 is listed in Table 1, but based on error that is bigger than 100 %, we are not able to draw any conclusions about interaction between particles.

From the Zimm plots, it was evident that the apparent R_G was under the evaluation limit at the highest micelle concentrations (2.12 g/L), while it increased considerably with dilution, and the extrapolated values reached around 60-65 nm (see Table 1). It would mean that the micelles did not disassemble in dilute solutions as usual for block copolymer micelles. There are two explanations: (i) the micelles change their morphology with dilution, or more probable (ii) the dilution introduced dust and a certain fraction of undefined aggregates. To distinguish which scenario is valid, further DLS and microscopy experiments were carried out.

From the dynamic Zimm plots (Figure 8), we were able to obtain the value of z-averaged diffusion coefficient, D_Z, as well as the value of hydrodynamic radius, R_H, using Stokes-Einstein equation (Equation 9). The values are summarized in Table 2.

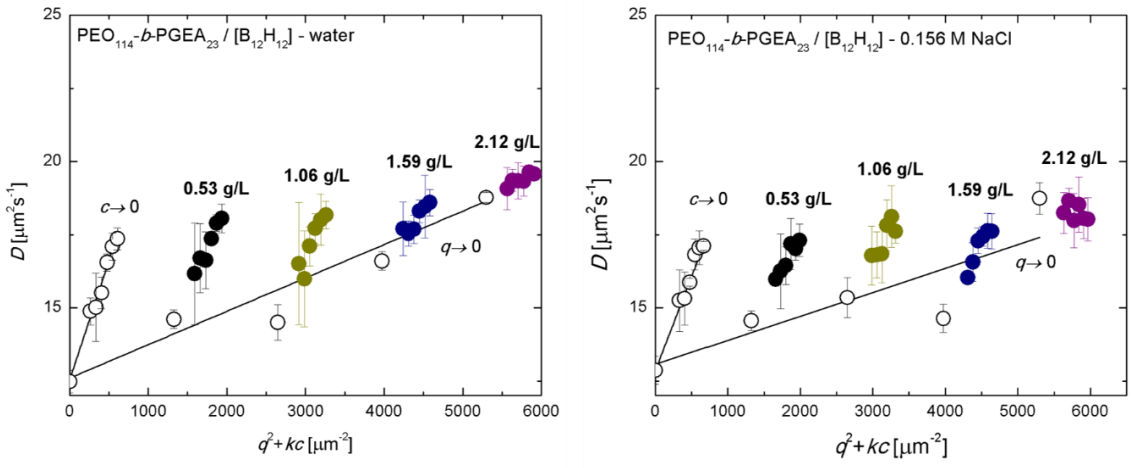

Figure 8: Dynamic Zimm plots of PEO_{114}-b-$PGEA_{23}$ /$[B_{12}H_{12}]$ in pure water and in 0.156M NaCl solution.

Table 2: Evaluation of dynamic Zimm plots of PEO_{114}-b-$PGEA_{23}$/$[B_{12}H_{12}]$ micelles in water and 0.156 M NaCl solution, where R_H is hydrodynamic radius and D_Z is z-averaged diffusion coefficient.

Sample	D_Z **[μm²/s]**	R_H **[nm]**
PEO-PGEA - water	12.48 ± 1.07	19
PEO-PGEA - salt	12.87 ± 1.89	18

As seen in Table 2, the micelles in water and in salt solution exhibit very similar diffusion coefficient, based upon these values we can presume that nanoparticles in pure water and in 0.156 M NaCl solution are approximately the same size. This assumption is further supported by values of hydrodynamic radius, R_H, also listed in Table 2. To obtained R_H values from dynamic Zimm plots the cumulant method was used. From the dynamic Zimm plots in Figure 8, it is evident that the q-dependence of apparent diffusion coefficients is more pronounced for dilute samples and almost no such dependence is observed for the sample with the highest concentration. It indicates the uniformity of the micelles decreased with dilution.

To reveal the changes in the size distribution upon a dilution as observed in both static and dynamic Zimm plots (Figures 7 and 8), we carried out the constrained inverse Laplace transform routine, CONTIN, at 90° scattering angle. The results for the micelles of the highest concentrations in water and 0.156 M NaCl are shown in Figure 9. Both distributions display monomodal character. The size distribution shows that values of R_H are roughly the same for nanoparticles in water and in salt solution, and that the micelles formed by PEO_{114}-*b*-$PGEA_{23}$/$[B_{12}H_{12}]^{2-}$ only consist of one population of nanoparticles.

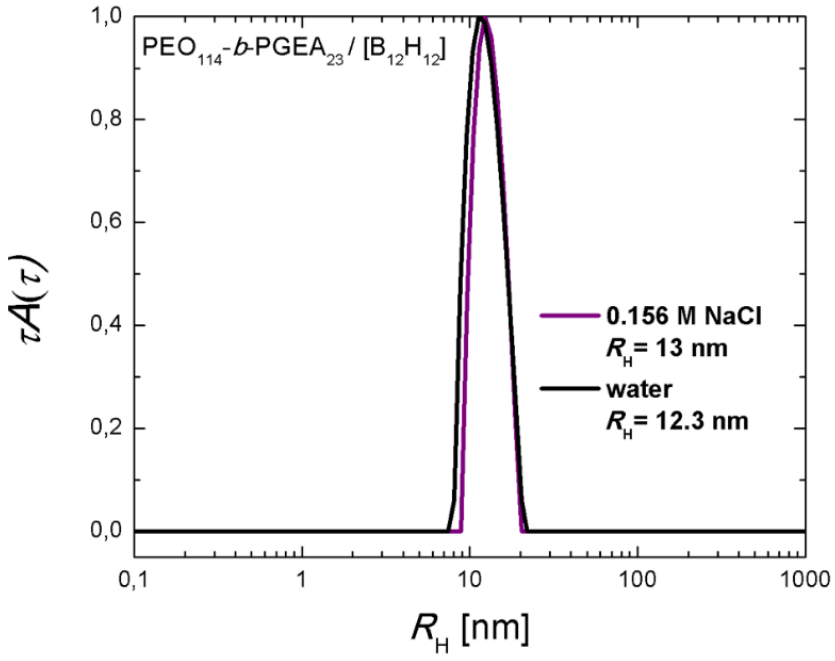

Figure 9: CONTIN analysis of PEO_{114}-b-$PGEA_{23}$/$[B_{12}H_{12}]$ samples in pure water and in 0.156 M NaCl solution at concentrations 2.12 g/L and scattering angle 90°.

The CONTIN analysis for dilute samples (not shown) revealed the presence of the slow mode, which corresponds to very small fraction of impurities and micellar aggregates with radii around 250-1000 nm. It means that the values of R_G and R_H obtained from static and dynamic Zimm plots (Figures 7 and 8, and Tables 1 and 2) are obscured by the presence of undefined impurities. Therefore, the hydrodynamic radius of the coassembled micelles obtained from the dynamic Zimm plot (around 20 nm) is overestimated and is close to the values obtained from the CONTIN analysis are more reliable (around 13 nm in both water and 0.156 M solution). The true value of radius of gyration of the micelles is under the limit of SLS, and, again, the values obtained from the Zimm plots

were not taken into the account. Thus the value of R_G/R_H could not be obtained for the studied systems.

5.2.2. Nuclear magnetic resonance

^{1}H NMR spectroscopy was used for tracking of the micelle formation during the addition of dodecaborate to P2VP$_{129}$-*b*-PEO$_{477}$ and PEO$_{114}$-*b*-PGEA$_{23}$ cationic diblock copolymer solutions. It has been shown that the signal of segments involved in the complex formation with anionic boron clusters is not visible in NMR spectrum. [Attachment A] It allows for the calculation of the fraction of free and frozen polymer segments during the coassembly process.

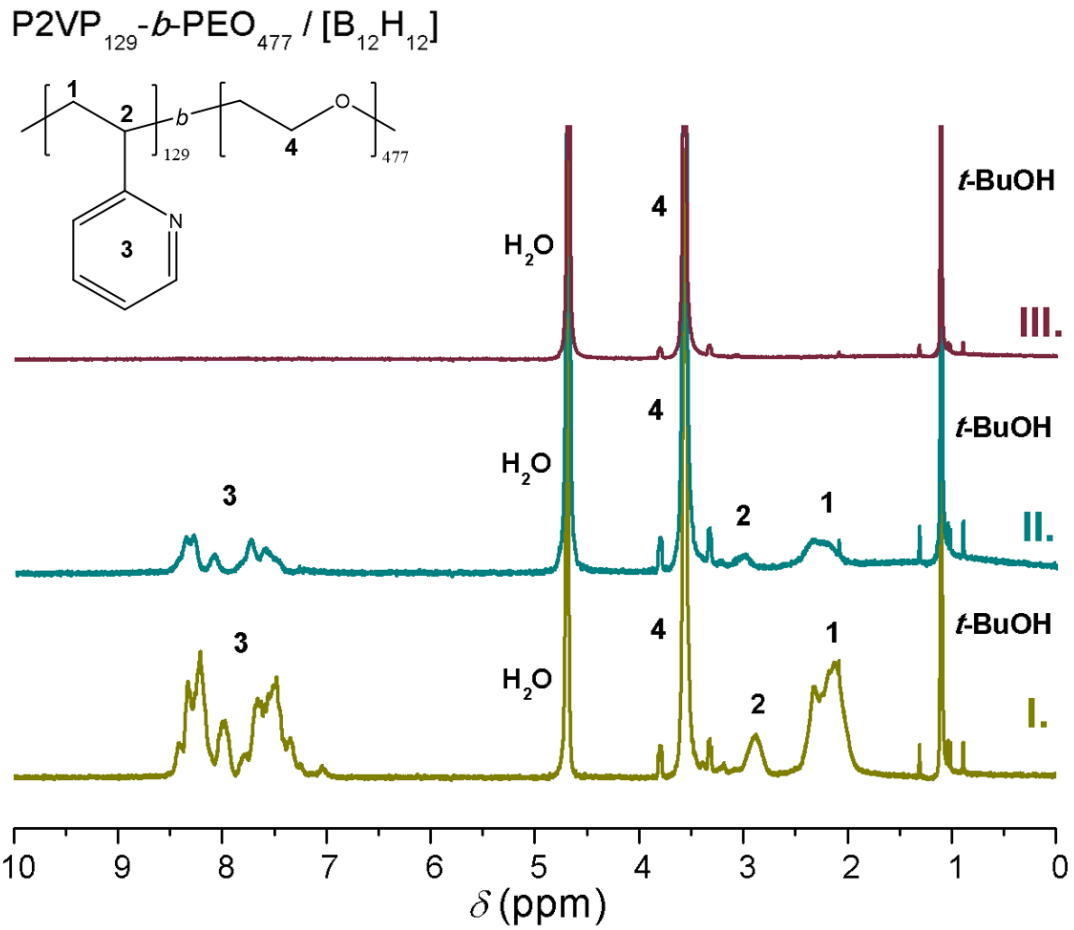

Figure 10: ^{1}H NMR spectra: I. [$B_{12}H_{12}$]/ P2VP$_{129}$-b-PEO$_{477}$ ratio 0.00, II. [$B_{12}H_{12}$]/ P2VP$_{129}$-b-PEO$_{477}$ ratio 0.50, III. [$B_{12}H_{12}$]/ P2VP$_{129}$-b-PEO$_{477}$ ratio 0.80. Signal assignments are shown in the block copolymer structure; t-BuOH was used as internal standard.

Sodium dodecaborate solution was added to P2VP$_{129}$-*b*-PEO$_{477}$ in DCl aqueous solution to obtain dodecaborate/pyridine ratios 0.00, 0.15, 0.30, 0.50, 0.80 and 1.00 (further details in

section 4.2.) and after each addition ^{1}H NMR spectrum has been measured (selected spectra for the ratios 0.00, 0.50 and 0.80 are shown in Figure 10).

With dodecaborate addition (spectra II. and III. In Figure 10), the relative intensity of CH_2 signal (peak **1**), CH signal (peak **2**) and signal of aromatic circle (peak **3**), which all correspond to the P2VP block, decreased. For dodecaborate/P2VP ratio 0.80 (spectrum III.) all three signals (peaks **1**, **2** and **3**) were not detectable at all. We can conclude that for ratios 0.80 and 1.00, all the core-forming segments are completely immobilized. Decreasing trend of relative intensity of P2VP unit for all ratios is presented in Figure 11. From Figure 11 we can see that even for dodecaborate/P2VP ratio 0.15 almost half of the core forming segments is immobilized. In contrast, the signal of PEO block (peak **4**) is not affected by dodecaborate addition. It means that only cationic segments are involved in the nanoparticle formation and the PEO blocks create the corona stabilizing the micelles in solution.

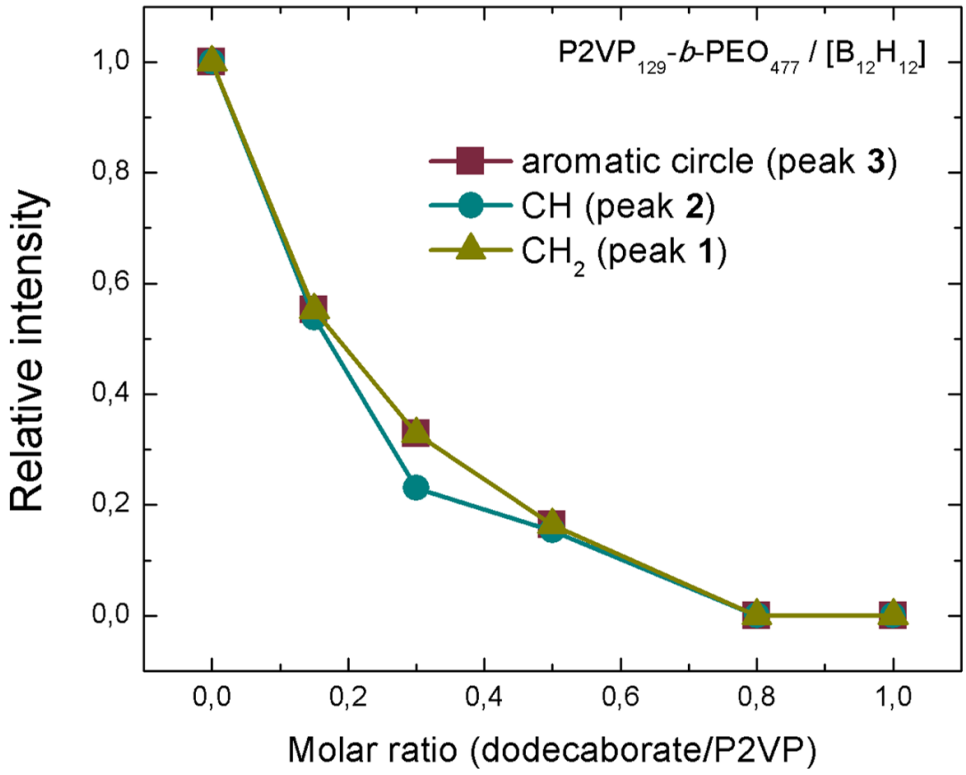

Figure 11: ^{1}H NMR relative intensity of P2VP unit for CH_2 signal, CH signal and signal of aromatic circle.

We carried out the same NMR titrations also with PEO-*b*-PGEA block copolymers (see Figure 2b in [Attachment A]). While the trend is similar as for $P2VP_{129}$-*b*-PEO_{477}, the fraction of frozen PGEA segments is less than 50% in saturated nanoparticles.

5.2.3. Cryo-TEM

From cryo-TEM imaging, we are able to obtain morphology of the PEO_{114}-*b*-$PGEA_{23}/[B_{12}H_{12}]$ nanoparticles. The cryo-TEM micrograph of the micelles for the dodecaborate/guanidine ratio = 0.5 in pure water is presented in Figure 12. From cryo-TEM micrographs we can observe spherical shape of nanoparticles that correspond to the values obtained by dynamic light scattering data (see the section 5.2.1). However, we should keep in mind that cryo-TEM usually visualize only the core of the micelles, while the hydrodynamic radius also includes the micellar corona with the hydration shell.

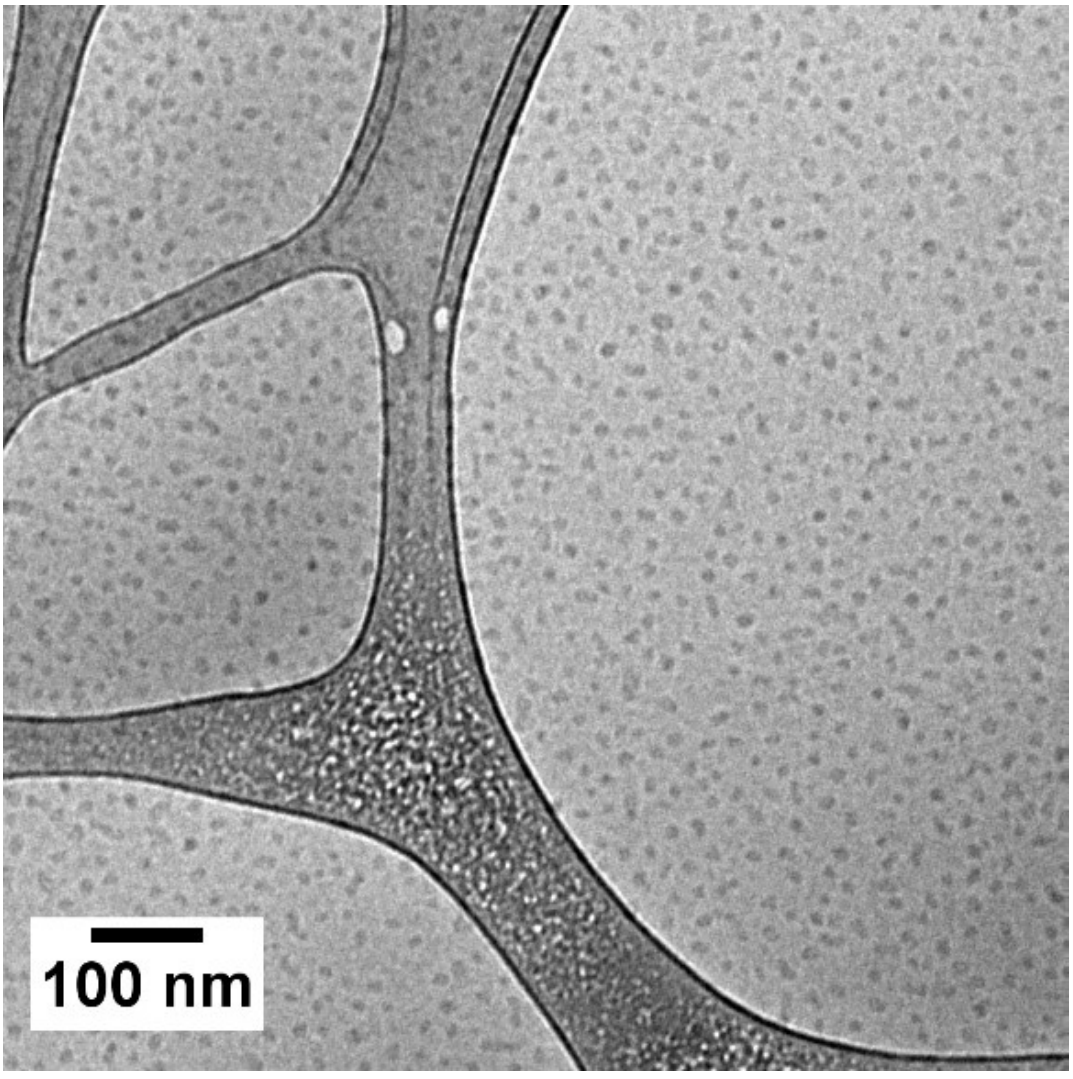

Figure 12: Typical cryo-TEM micrograph of PEO_{114}-b-$PGEA_{23}/[B_{12}H_{12}]$ in water; the nanoparticles are visualized as small grey spherical objects.

6. Conclusion

The stable boron-rich nanoparticles of spherical shape were prepared by coassembly of cationic diblock copolymer PEO_{114}-*b*-$PGEA_{23}$ with anionic boron cluster compound dodecaborate, $[B_{12}H_{12}]^{2-}$, in water and 0.156 M NaCl solution. Size, shape and mechanism of formation of the micelles were studied by static and dynamic light scattering, NMR spectroscopy and cryo-TEM imaging.

The cationic diblock copolymer $P2VP_{129}$-*b*-PEO_{477} in HCl aqueous solutions also formed nanoparticles with dodecaborate. Due to low particle uniformity and instability in solution, the samples were not studied by light scattering techniques and only NMR titrations were carried out.

The light scattering and NMR spectroscopy titration experiments confirmed that the nanoparticles formation was based on interaction of cationic PGEA and P2VP blocks with dodecaborate anions leading to the core-corona micelles with the dodecaborate complex in the core shielded by the PEO corona. After the saturation around the dodecaborate/guanidine ratio 0.25-0.5, the PEO_{114}-*b*-$PGEA_{23}$/$[B_{12}H_{12}]$ micelles did not further change their size and morphology.

The aggregation number of the saturated PEO_{114}-*b*-$PGEA_{23}$/$[B_{12}H_{12}]$ micelles (dodecaborate/guanidine ratio = 0.5) in water and 0.156 M NaCl solution was determined by standard Zimm technique. Prior the light scattering measurements, the values of $\frac{dn}{dc}$ were determined by using of refractometry. The numbers of PEO_{114}-*b*-$PGEA_{23}$ chains in the micelles were calculated as 47 ± 13 and 37 ± 7 in water and 0.156 M NaCl solution, respectively. It means that the aggregation number slightly decreased with ionic strength, probably due to impact of salt on dodecaborate-guanidine interaction.

7. References

1. Keddie, Daniel J. A guide to the synthesis of block copolymers using reversible-addition fragmentation chain transfer (RAFT) polymerization. *Chem. Soc. Rev.*, 2014, 43, 496-505; doi:10.1039/C3CS60290G.
2. Zhou, J.; Yao, H.; Ma, J. Recent advances in RAFT-mediated surfactant-free emulsion polymerization. *Polym. Chem.*, 2018, 9, 2532-2561; doi:10.1039/C8PY00065D.
3. Tian, X.; Ding, J.; Zhang, B.; Qiu, F.; Zhuang, X.; Chen, Y. Recent Advances in RAFT Polymerization: Novel Initiation Mechanisms and Optoelectronic Applications. *Polymers,* 2018, 10, 318; doi:10.3390/polym10030318.
4. Rieger J.; Stoffelbach F.; Bui C.; Alaimo D.; Jérôme C.; Charleux B. Amphiphilic Poly(ethylene oxide) Macromolecular RAFT Agent as a Stabilizer and Control Agent in ab Initio Batch Emulsion Polymerization. *Macromolecules,* 2008, 41, 4065-4068; doi:10.1021/ma800544v.
5. Nagarajan, R. Amphiphilic surfactants and amphiphilic polymers: Principles of molecular assembly. *ACS Symposium Series*, 2011, Chapter 1, pp 1-22; doi:10.1021/bk-2011-1070.ch001.
6. Weiss, P. Block copolymers – overview and critical survey, Allen Noshay and James E. Mcgrath, Academic, New York. *J.*, *Polym. Sci. B Polym. Lett. Ed.*, 1978, 516 pp; doi:10.1002/pol.1978.130160313.
7. Tritschler, U.; Pearce, S.; Gwyther, J.; Whittell, G. R.; Manners, I. 50th Anniversary Perspective: Functional Nanoparticles from the Solution Self-Assembly of Block Copolymers. *Macromolecules*, 2017, 50, 3439-3463; doi:10.1021/acs.macromol.6b02767.
8. Borisov O. V.; Zhulina E. B. Morphology of micelles formed by diblock copolymer with a polyelectrolyte block, *Macromolecules*, 2003, 36, 10029-10036; doi:10.1021/ma0304628.
9. Berret J.-F. Controlling electrostatic co-assembly using ion-containing copolymers: From surfactants to nanoparticles. *Advances in Colloid and Interface Science*, 2011, 167, 38-48; doi:10.1016/j.cis.2011.01.008.
10. Matějíček Pavel Erratic ions: self-assembly and coassembly of ions of nanometer size and of irregular structure. *Current Opinion in Colloid & Interface Science*, 2020, 45, 97-107; doi:10.1016/j.cocis.2019.12.008.

11. Fernandez-Alvarez R.; Ďorďovič V.; Uchman M.; Matějíček P. Amphiphiles without head-and-tail design: Nanostructures based on the self-assembly of anionic boron cluster compounds. *Langmuir*, 2018, 34, 3541-3554; doi:10.1021/acs.langmuir.7b03306.
12. Ekholm V.; Vazdar M.; Manson P. E.; Bialik E.; Walz M-M.; Öhrwall G.; Werner J.; Rubensson J-E.; Jungwirth P.; Björneholm O. Anomalous surface behavior of hydrated guanidinium ions due to ion pairing. *J. Chem. Phys.*, 2018, 148, 144508; doi:10.1063/1.5024348.
13. Kolonko E.M.; Kiessling L.L. A polymeric domain that promotes cellular internalization. *J Am Chem Soc*. 2008, 130, 5626-5627; doi:10.1021/ja8001716.
14. Koltzenburg, S.; Maskos M. Nuyken O. Polymer chemistry. Berlin: Springer Verlag, 2017; ISBN 978-3-662-49277-2.
15. Munk P.; Aminabhavi T. M. Introduction to macromolecular science. 2nd ed. New York: Wiley, 2002; ISBN 0-471-41716-5.
16. Schärtl W. Light scattering from polymer solutions and nanoparticle dispersions; Springer: Berlin, 2010; ISBN 978-3-540-71951-9.
17. Øgendal, L. H. Light Scattering Demystified: Theory and Practice; University of Copenhagen, Denmark, 2017.
18. Stetefeld J.; McKenna S.A.; Patel T.R. Dynamic light scattering: a practical guide and applications in biomedical sciences. *Biophys Rev*. 2016, 8, 409-427; doi:10.1007/s12551-016-0218-6.
19. Hatada, K.; Kitayama, T. NMR Spectroscopy of Polymers; Springer-Verlag Berlin Heidelberg, 2004; ISBN 978-3-662-08982-8.
20. Hore, P. J.; Jones, J. A.; Wimperis S. NMR: The toolkit; Oxford ; New York : Oxford University Press, 2000; ISBN: 9780198703426.
21. Martin L.; Peltier R.; Kuroki A.; Town J. S.; Perrier S. Investigating cell uptake of guanidinium-rich RAFT polymers: Impact of comformer and monomer distribution. *Biomacromolecules*, 2018, 19, 3190-3200; doi:10.1021/acs.biomac.8b00146.
22. Liu J.; Ai X.; Zhang H.; Zhuo W.; Mi P. Polymer micelles with Endosome escape and erdox-responsive functions for enhanced intracellular drug delivery. *Journal of Biomedical Nanotechnology*, 2019, 15, 373-381; doi:10.1166/jbn.2019.2693.
23. Tibbitt, M. W.; Dahlman, J. E.; Langer, R. Emerging frontiers in drug delivery. *J. Am. Chem. Soc.*, 2016, 138, 704-717; doi:10.1021/jacs.5b09974.

24. Yura Y.; Fujita Y. Boron neutron capture therapy as a novel modality of radiotherapy for oral cancer: Principle and antitumor effect. *Oral Science International*, 2013, 10, 9-14; doi:10.1016/S1348-8643(12)00046-8.
25. Kuthala N.; Vankayala R.; Li Y. N.; Chiang C.S.; Hwang K. C. Engineering novel targeted boron-10-enriched theranostic nanomedicine to combat against murine brain tumors via MR imagining-guided boron neutron capture therapy. *Adv. Mater*, 2017, 29, 1700850; doi:10.1002/adma.201700850.
26. Lai J. T.; Filla D.; Shea R. Functional polymers from novel carboxyl-terminated trithiocarbonates as highly efficient RAFT agents. *Macromolecules*, 2002, 35, 6754-6756; doi:10.1021/ma020362m.
27. Wang Rui-Yang, Xu Jun-Ting, Du Bin-Yang, Fan Zhi-Qiang, et al. Design and regulation of lower disorder-to-order transition behavior in the strongly interacting block copolymers. *Macromolecules*, 2018, 51, 2302-2311; doi:10.1021/acs.macromol.8b00227.

Appendix

Attachment A: Paper

Designed Boron-Rich Polymeric Nanoparticles Based on Nano-Ion Pairing for Boron Delivery
Li Jianwei, Janoušková Olga, Fernandez-Alvarez Roberto, Mesíková Soňa, Tošner Zdeněk, Kereïche Sami, Mariusz Uchman and Matějíček Pavel
Chem. Eur. J., 2020; doi: 10.1002/chem.202001699